Int. J. Morphol.,
43(2):458-469, 2025.

Protective Effects of Probiotics and Mesalazine Against Capecitabine-Induced Enterocolitis in Rats: A Comprehensive Biochemical, Molecular, Stereological and Histopathological Investigation

Efectos Protectores de los Probióticos y la Mesalazina Contra la Enterocolitis Inducida por Capecitabina en Ratas: Una Investigación Bioquímica, Molecular, Estereológica e Histopatológica

Hao Che[1]; Yuejun Xu[1]; Yafan Huang[1] & Zhiwei Guo[1]

CHE, H.; XU, Y.; HUANG, Y. & GUO, Z. Protective effects of probiotics and mesalazine against capecitabine-induced enterocolitis in rats: A comprehensive biochemical, molecular, stereological, and histopathological investigation. *Int. J. Morphol., 43 (2)*:458-469, 2025.

SUMMARY: This study aimed to explore the protective effects of a probiotic mixture (PrM) consisting of *Lactobacillus casei*, *Lactobacillus rhamnosus*, and Lactobacillus helveticus, along with Mesalazine (MZ), against Capecitabine (CT)-induced enterocolitis. The investigation was conducted using a combination of biochemical, molecular, and histopathological analyses. Fifty Wistar rats were randomly assigned to five groups (10 rats each) and monitored over a 50-day period. The groups included a sham group, a CT-only group, a group receiving CT and MZ (50 mg/kg), a group receiving CT and PrM (10 mg/kg), and a co-treatment group receiving CT, MZ, and PrM. On day 51, following euthanasia, blood samples were collected from the hearts of the rats for further analysis. Serum nitric oxide levels, as well as the activity of antioxidant enzymes such as catalase, glutathione peroxidase, and superoxide dismutase, were measured. Serum concentrations of antidiuretic hormone (ADH) and arginine vasopressin (AVP) were also assessed. Oxidative stress markers in intestinal tissue, including FRAP, thiol, and TBARS, were evaluated. Pro-inflammatory cytokine levels, such as interleukin-6 (IL-6), tumor necrosis factor-a (TNF-α), interleukin-1β (IL-1β), and IL-10 were quantified using ELISA. Water homeostasis in the intestine was investigated by examining the expression of aquaporin's (AQP) (AQP3, AQP8, and AQP6) genes through real-time PCR, while protein expression was determined using western blotting. Additionally, the structural integrity of intestinal tissue across the study groups was assessed through histopathological evaluation. Both MZ and PrM treatments were found to reduce intestinal cell apoptosis and up-regulate the expression of intestinal AQPs genes and proteins by enhancing antioxidant enzyme activity and reducing free radical levels. The combined treatment also demonstrated a synergistic effect in modulating pro-inflammatory cytokine levels and regulating ADH and AVP, contributing to the maintenance of serum and intestinal osmotic balance. The study suggests that MZ and PrM have potential therapeutic benefits for managing enterocolitis in patients undergoing chemotherapy by mitigating oxidative stress, reducing inflammation, and preserving intestinal water homeostasis.

KEY WORDS: Probiotic; Mesalazine; Capecitabine; Intestine; Enterocolitis; Apoptosis.

INTRODUCTION

Chemotherapy-induced enterocolitis (CIE) is a recognized complication of cancer treatment, characterized by symptoms like abdominal pain, diarrhea, nausea, and weight loss. The mechanisms behind CIE are complex and not fully understood, but several key processes have been identified (Zhan *et al*., 2023). Chemotherapy agents damage intestinal epithelial cells, compromising the intestinal barrier and increasing permeability, which allows bacteria and toxins to enter. This leads to inflammation through immune cell activation and the release of pro-inflammatory cytokines, resulting in further tissue damage. Additionally, chemotherapy induces oxidative stress by disrupting the balance between reactive oxygen species (ROS) and antioxidants, causing further cellular harm. It also alters gut microbiota, leading to dysbiosis, which exacerbates inflammation (Wang *et al*., 2021). The regenerative capacity of intestinal epithelial cells is impaired, prolonging inflammation and contributing to abnormal immune responses against intestinal tissues. Aquaporins (AQPs), integral membrane proteins that regulate water transport, are

[1] Department of Anorectal, Wuhan Eighth Hospital (Wuhan Anorectal Hospital), Wuhan, China.

Received: 2024-10-03 Accepted: 2024-12-22

negatively affected by chemotherapy. Disruption of AQP function can disturb water homeostasis and intestinal barrier integrity, further contributing to inflammation. Specifically, AQP3 and AQP8 play roles in immune responses and tissue repair, and any alterations in their expression can hinder healing processes (Li *et al*., 2024).

Capecitabine (CT) is a commonly used oral chemotherapy drug for various cancers, including breast and colorectal cancer. While effective, it can cause gastrointestinal side effects such as diarrhea and nausea. CT is converted into its active form, fluorouracil (5-FU), which disrupts RNA and DNA synthesis, leading to cell death (Alzahrani *et al*., 2023). The mechanisms of CT-induced enterocolitis likely involve immune dysregulation, oxidative stress, and direct toxicity to the intestinal lining. Research indicates that CT metabolites activate several molecular pathways associated with inflammation and apoptosis, contributing to the development of CIE. Additionally, bioactive compounds from plant extracts may help protect normal cells from the damaging effects of chemotherapy, potentially enhancing therapeutic outcomes (Agrawal *et al*., 2024).

Mesalazine (MZ), or 5-aminosalicylic acid (5-ASA), is an anti-inflammatory medication primarily used to treat inflammatory bowel diseases (IBD) such as ulcerative colitis and Crohn's disease. It is a derivative of salicylic acid with the chemical formula C7H7N3O3S (S?oka *et al*., 2023). Historically, salicylates have been utilized for their anti-inflammatory properties, and while MZ is not a traditional herbal remedy, it follows the principles of using anti-inflammatory agents for digestive issues. In modern medicine, MZ is a first-line treatment for inducing and maintaining remission in mild to moderate ulcerative colitis and Crohn's disease, often used post-surgery to prevent recurrence. It acts topically on the colonic mucosa, inhibiting pro-inflammatory cytokines, reducing oxidative stress, and modulating immune responses (Beiranvand, 2021). Clinical trials have demonstrated its efficacy and safety, with common side effects being gastrointestinal disturbances and headache (D'amico *et al*., 2019). Animal studies exhibit the ability to hinder the activation of nuclear factor-kappa B (NF-kB), a pivotal mediator of inflammation, and suppress the expression of inflammatory enzymes like cyclooxygenase-2 (COX-2) and inducible nitric oxide synthase (iNOS) in enterocytes during chemotherapy (Beiranvand & Bahramikia, 2020). Through the reduction of oxidative stress, MZ provide protection against intestinal damage and inflammation. Moreover, they stimulate the production of anti-inflammatory cytokines while dampening the release of pro-inflammatory cytokines, thus fostering immune balance and alleviating inflammation.

Probiotic mixtures (PrM) have demonstrated potential benefits for gastrointestinal health, particularly in managing conditions like ulcerative colitis and enterocolitis. These probiotics enhance gut health by improving digestion, modulating immune responses, and promoting mucosal healing while restoring gut microbiota balance (Gu *et al*., 2022). They exert their effects through various molecular pathways, including the regulation of apoptosis, inhibition of the NF-kB pathway to reduce inflammation, modulation of the MAPK pathway, and activation of the PI3K/Akt/mTOR pathway to promote cell survival and growth (Dashtbanei & Keshtmand, 2023). Clinical studies in humans and animal models have shown that these probiotics can alleviate symptoms, reduce inflammatory markers, and improve overall quality of life, indicating their promise in therapeutic applications, although further research is needed to clarify their mechanisms and optimize use (Han *et al*., 2021). The aim of our study was to explore the potential protective and therapeutic effects of probiotics (*Lactobacillus casei*, *Lactobacillus rhamnosus*, and *Lactobacillus helveticus*) and MZ in relation to CT-induced enterocolitis (CIE) in rats. We utilized biochemical, molecular, and histopathological methods to assess the impact of MZ and probiotic mixtures on CIE.

MATERIAL AND METHOD

PrM and MZ preparation

Mesalazine (CAS 89-57-6, Sigma, USA), which releases 5-ASA throughout the intestinal tract, was introduced into a Nelaton catheter (Terumo, Tokyo, Japan) and subsequently injected into the stomach using a 0.5% sodium carboxymethylcellulose solution at a daily dosage of 100 mg/kg (Beiranvand & Bahramikia, 2020).

A powdered blend of probiotics, comprising *Lactobacillus rhamnosus* (IBRC-M11322), *Lactobacillus helveticus* (TG-35), and *Lactobacillus casei* (IBC-M10784), was sourced from Techgen Bio (Techgen Bio, Malaysia) at a concentration of 10∂? CFU/ml. To create the solution, 1 ml of this probiotic mixture was mixed with 9 ml of distilled water, yielding a final concentration of 1x10? CFU/ml (Dashtbanei & Keshtmand, 2023).

Animals and experimental design

Before the study began, the rats underwent a 72-hour acclimatization period to adapt to their experimental environment. Any rats exhibiting signs of illness, particularly gastrointestinal issues like diarrhea and anorexia, were excluded from the study. The research adhered to international guidelines, protocols, and ethical standards

established by the Wuhan Eighth Hospital (Wuhan Anorectal Hospital) ethics committee. The rats were kept in controlled laboratory conditions, with a temperature of 25±3 °C, relative humidity of 45±4 %, and a 12-hour light/dark cycle, while having ad libitum access to standard rodent pellets and tap water. A total of 50 adult male Wistar rats, each weighing between 220±30 g, were then divided into five groups for observation over 50 days.

The groups included a sham group that received 1 ml of distilled water orally, a CT group that received 500 mg/kg of CT orally, a PrM treatment group (CT + PrM) that received CT along with 10 mg/kg of PrM orally, an MZ treatment group (CT + MZ) that received CT with 100 mg/kg of MZ orally, and a co-treatment group (CT + PrM + MZ) that received CT, 100 mg/kg of MZ, and 10 mg/kg of PrM orally (Beiranvand & Bahramikia, 2020; Dashtbanei & Keshtmand, 2023; Li *et al*., 2024).

A pilot studies and similar research involving CT, PrM, and MZ, was used to establish a non-toxic effective dose. Throughout the study, CT, PrM, and MZ were administered daily at specific intervals: CT at 9 am, PrM at 3 pm, and MZ at 9 pm.

Arginine vasopressin (AVP) and antidiuretic hormone (ADH) serum levels

At the end of the study, after euthanizing the rats with pre-anesthesia and anesthesia using 50 mg/kg xylazine (2%) and 30 mg/kg ketamine (10 %), blood samples were collected from the heart, and serum samples were separated through centrifugation. The serum concentrations of ADH (catalog number: E-EL-H0272, Elabscience, USA) and AVP (catalog number: MBS700417, MyBioSource, USA) were measured using commercial ELISA kits following the manufacturer's guidelines (Golosova *et al*., 2019).

Superoxide dismutase (SOD), catalase (CAT), and glutathione peroxidase (GPx) serum activity

To assess GPx activity, we followed the manufacturer's guidelines for a Cell Signal ELISA kit. Serum samples underwent lysis with 100 µl of buffer in a 96-well plate, incubated for 10 min at 4 °C, and then centrifuged at 10,000 rpm for 5 min. The supernatant was transferred to a new plate, where 50 µl of the working solution and assay buffer were added. After a 10 min incubation at 37 °C and centrifugation, absorbance was measured at 450 nm using a UV-visible spectrophotometer (Li *et al*., 2024).

For SOD activity, we utilized an Elabscience ELISA kit. Fifty µl of serum samples and standards were added to wells, followed by 50 µl of primary antibody and 100 µl of conjugated horseradish peroxidase (HRP). After a 30 min incubation at 37 °C, we added stop and substrate solutions, followed by another 15 min incubation before measuring absorbance at 450 nm (Meshkibaf *et al*., 2019).

To measure CAT activity, we employed another Elabscience ELISA kit. We added 100 µl of serum samples and standards to wells and incubated for 2 h at 25 °C with shaking. We then added 100 µl of a biotinylated antibody, followed by an hour of incubation. Next, 100 µl of streptavidin solution were added, and after a 45 min incubation, 100 µl of TMB substrate reagent was introduced. Absorbance was measured at 450 nm after a final 30 min dark incubation at 25 °C (Meshkibaf *et al*., 2019).

Serum levels of nitric oxide (NO)

The serum levels of nitric oxide (NO), an indicator of free radical production, were quantified using the ZellBio ELISA kit in accordance with the manufacturer's guidelines. Initially, 50 µl of serum and standard samples, pre-diluted in assay buffer, were added to the wells of a 96-well plate. Following this, 10 µl of nitric reductase solution was introduced to each well. The mixture was incubated for 20 min at 37 °C, after which 25 µl of solutions A and B from the kit were added. Another incubation period of 20 min at 37 °C followed. Finally, the absorbance of the mixture was measured at 540 nm and 570 nm using a UV-visible spectrophotometer (Model No. V-630 Bio; JASCO, US) (Yarahmadzehi *et al*., 2020).

Intestine FARP, total thiol, and TBARS levels

The total antioxidant capacity was assessed using the ferric reducing ability of plasma (FRAP) assay, where 100 mg of tissue was homogenized with 200 µl of cold PBS, and 100 µl of this mixture was combined with 10 µl of FRAP solution. After incubating for 15 min at 25 °C and centrifuging at 12,000 rpm for 10 min, the absorbance was measured at 593 nm using a UV-visible spectrophotometer (Li *et al*., 2024).

Lipid peroxidation was quantified by measuring thiobarbituric acid reactive substances (TBARS). In this step, 100 µl of homogenized intestinal tissue was mixed with 100 µl of TBARS solution, incubated for 30 min at 37 °C, and centrifuged. The absorbance of the supernatant was then measured at 593 nm (Xiao *et al*., 2024).

To evaluate tissue thiol levels, an important antioxidant capacity marker, 100 µl of the homogenized intestinal tissue was mixed with 20 µl of 5,5'-dithio-bis-(2-

nitrobenzoic acid) (DTNB). After a 15 min incubation at 37°C and centrifugation, absorbance was measured at 412 nm (Yarahmadzehi *et al*., 2020).

IL-10, IL-1β, IL-6, and TNF-α serum levels

To evaluate the serum levels of pro- and anti-inflammatory cytokines, commercial ELISA kits from R&D Systems, Inc. were utilized in accordance with the manufacturer's instructions. The procedure began with the addition of 50 µL of Assay Diluent RD1-54 into each well of a 96-well plate, followed by the introduction of 50 µL of standard, control, or sample into the corresponding wells. After a 2 h incubation at room temperature, 100 µL of Rat IL-6 Conjugate was added to each well, along with 100 µL of Substrate Solution. The mixture was then incubated for an additional 30 min at room temperature. Following this, 100 µL of Stop Solution was added to each well, and the resulting mixture was allowed to sit for another 30 minutes. Finally, the absorbance of the solution was measured at 540 nm using a UV-visible spectrophotometer (Model No. V-630 Bio; JASCO, US) (Zogbi *et al*., 2020).

Intestine total RNA extraction and AQP3, AQP8, and AQP6 genes expression with quantitative Real-Time PCR (qPCR)

The extraction of total RNA from 50 mg of intestinal tissue was accomplished using the Canvas Biotech Total RNA Purification Kit. Initially, the tissue was homogenized and treated with Buffer BLY in combination with b-mercaptoethanol. Following this treatment, the mixture was centrifuged to separate the supernatant, which was then passed through a filter column and washed with 70 % ethanol. The isolated RNA pellet was then suspended in deionized water and stored at -70 °C. The concentration of RNA was determined using a Nanodrop spectrophotometer, while its quality was evaluated through 2 % agarose gel electrophoresis. For cDNA synthesis, 1 mg of the extracted RNA was mixed with the qScriber reaction master mix, deionized water, and specific primers, undergoing a designated temperature cycling protocol. Primer design was facilitated by Primer-3 software and subsequently verified using the NCBI database, with b-actin serving as the internal reference for measuring gene expression. Quantitative PCR (qPCR) was conducted using SYBR Green Master Mix, cDNA, and the specific primers for the target genes. This involved running 42 thermal cycles, during which the threshold cycle (CT) values for genes AQP6, AQP8, and AQP3 were recorded (primer sequences are listed in Table I). The relative expression of genes was then calculated using the ΔΔCt method:

Table I. Primer sequences.

Gene	Sequences (5´–3´)
β-actin	Forward: AGGCATCCTCACCCTGAAGTA
	Reverse: CACACGCAGCTCATTGTAGA
AQP3	Forward: GTGACAGGAAGAGCCAGGAG
	Reverse: TGAGGCTGAGCTTAGGGGTA
AQP8	Forward: GGAGCTGCCATGTCAAAGAT
	Reverse: CGCCCCTAGCAATACTACCA
AQP6	Forward: GGTGTTGGTGATCGGAGTCT
	Reverse: CGCCCTAAACACCTCATCC

AQP3, AQP8, and AQP6 proteins expression with western blotting

To evaluate the protein expression levels of AQP3, AQP6, and AQP8, Western blotting was performed. First, homogenized intestinal tissue samples were prepared, with 100 mg of tissue combined with 50 µl of PBS and 100 µl of radio-immunoprecipitation assay buffer. Following centrifugation, 20 µl of loading buffer was applied to a polyvinylidene fluoride (PVDF) membrane, which was then incubated with primary antibodies specific for AQP6 (Catalog number: ab191061; dilution 1:400, Abcam Bioscience, UK), AQP3 (Catalog number: EPR19932; dilution 1:500, Abcam Bioscience, UK), and AQP8 (Catalog number: AQP-008; dilution 1:200, Techne Corporation, R&D Systems, USA). Separation was conducted using a 10% SDS-polyacrylamide gel. After 12 h of incubation at 4°C, the membrane was incubated for 40 min at 37 °C with an HRP-conjugated secondary antibody. Protein band signals were then detected and analyzed using Bio-Rad software, with an enhanced chemiluminescence reagent from e-BLOT company, China, and further processed in Image J software (Cai *et al*., 2023).

Intestine stereology

To evaluate tissue damage and histopathological changes in the intestine across different experimental groups, intestinal tissue samples were collected and fixed in 10 % formalin. Following standard tissue processing, 5-micrometer-thick sections were prepared. These sections were stained with hematoxylin and eosin to visualize tissue structures. Morphological assessment of the intestinal layers—mucosa, submucosa, tunica muscularis, and serosa/adventitia—as well as lymphocyte infiltration levels, was performed using an optical microscope (Model BX61TRF; Olympus, Japan) equipped with a Moticam 1080N BMH camera system.

Fold change formula: 2-DDCT; where DDCt = [(Ct sample-Ct housekeeping gene) - (Ct sample-Ct control)] (Xiao *et al*., 2024).

The total volume of the intestine, as well as the volumes of its individual layers, were determined using Cavalieri's principle. Sections were selected based on systematic random sampling (SRS), with an interval between sections (designated as "t" in the Cavalieri method) randomly set to 200 µm, resulting in every 40th section being chosen for analysis. To estimate volumes, a point grid containing 81 crosses (+) was used. This grid was superimposed on section images, and the points overlaying the tissue sections were counted. Each point was conventionally marked at the upper right corner of the intersection point **(Fig. 1).** The total (absolute) volume of the intestine was then calculated using the formula:

$$V_{\text{total}} = \frac{\sum P \,.a/p.t}{M^2}$$

where "p" is the total number of points hitting the sections, "a/p" represents the area per point (100 mm^2), "t" is the interval between sections (200 µm or 0.2 mm), and "M" is the linear magnification.

The volume density (fractional volume) of the layers of the intestinal wall (including tunica mucosa, tunica submucosa, tunica muscularis, and tunica serosa/adventitia) was estimated with the following formula:

$$V_v = \frac{\sum P_{\text{structure}}}{\sum P_{\text{reference}}}$$

where "$P_{structure}$" is the total number of points hitting the desired structure, and "P reference" represents the points within the reference space.

The coefficient of error (CE) for the Cavalieri volume estimate was calculated using the following formula:

$$CE(V) = \frac{1}{\sum P}\left(\frac{1}{12}\{3a + c - 4b\}\right)^{1/2}$$

where, $a = \sum_{i=1}^{m} Pi.Pi$

$b = \sum_{i=1}^{m} Pi\,.\,Pi{+}1$

$c = \sum_{i=1}^{m} Pi.\,Pi{+}2$

subsequently, the coefficient error for fractional volume was estimated as follow:

$$CE(Vv) = \left[\frac{k}{k-1}\left\{\frac{\sum u^2}{\sum u.\sum u} + \frac{\sum v^2}{\sum v.\sum v} - 2\frac{\sum uv}{\sum u.\sum v}\right\}\right]^{1/2}$$

where, k was the number of sections, was the total points hitting the reference space and was tha sum of points hitting the desired structure (Goodarzi *et al*., 2019; Bojarzadeh *et al*., 2024; Loya-Zurita *et al*., 2024).

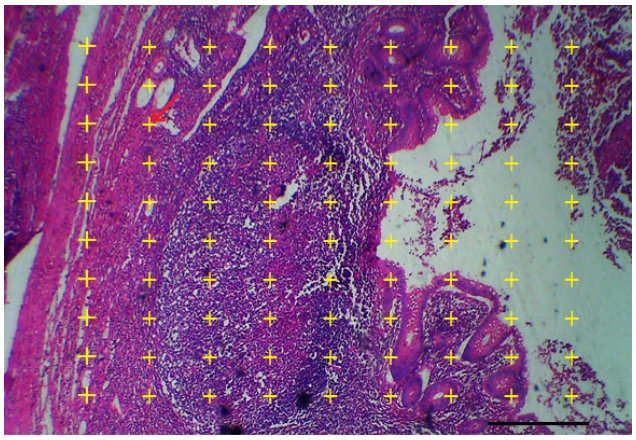

Fig. 1. The point counting method for volume estimation. The sum of the points hitting the desired structure (P structure) divided by the sum of the point hitting the section area (P reference) to obtain the volume density. The point was conventionally considered as the top right-hand corner (red arrow) of the crossing point. (H&E, Bar = 200 µm, 100×).

Statistical analysis approach. To compare quantitative results across the study groups, statistical analysis was performed using one-way analysis of variance (ANOVA), followed by the Newman-Keuls post hoc test. A p-value of less than 0.05 was deemed statistically significant. Data normality and homogeneity were verified with the Kolmogorov-Smirnov test, with a p-value above 0.05 indicating a normal distribution and uniformity among groups. Results are expressed as means ± standard deviation (SD). Data analysis was carried out using SPSS software (Version 16; IBM Inc., USA), while GraphPad Prism (Version 9; GraphPad Inc., USA) was used for generating visual representations.

RESULTS

Body weight. At the conclusion of the study, findings revealed that CT treatment led to a substantial decrease ($p < 0.01$) in rat weight compared to the sham group. In contrast, rats in the CT+MZ ($p < 0.05$) and CT+MZ+PrM ($p < 0.01$) groups, which received MZ and PrM, showed a synergistic effect, resulting in a significant weight increase compared to the CT group (Fig. 2a).

Serum levels of ADH and AVP. The analysis of serum ADH and AVP levels revealed a significant decrease ($p < 0.01$) in both markers in the CT group compared to the sham group. However, MZ treatment notably ($p < 0.05$) increased these serum parameters relative to the CT group. Additionally, PrM alone significantly elevated the serum level of AVP in the CT+PrM group ($p < 0.05$) compared to the CT group. The most pronounced changes in serum ADH and AVP levels were observed in the CT+MZ+PrM co-treatment group, where both serum markers increased significantly ($p < 0.01$) compared to the CT group (Fig. 2b).

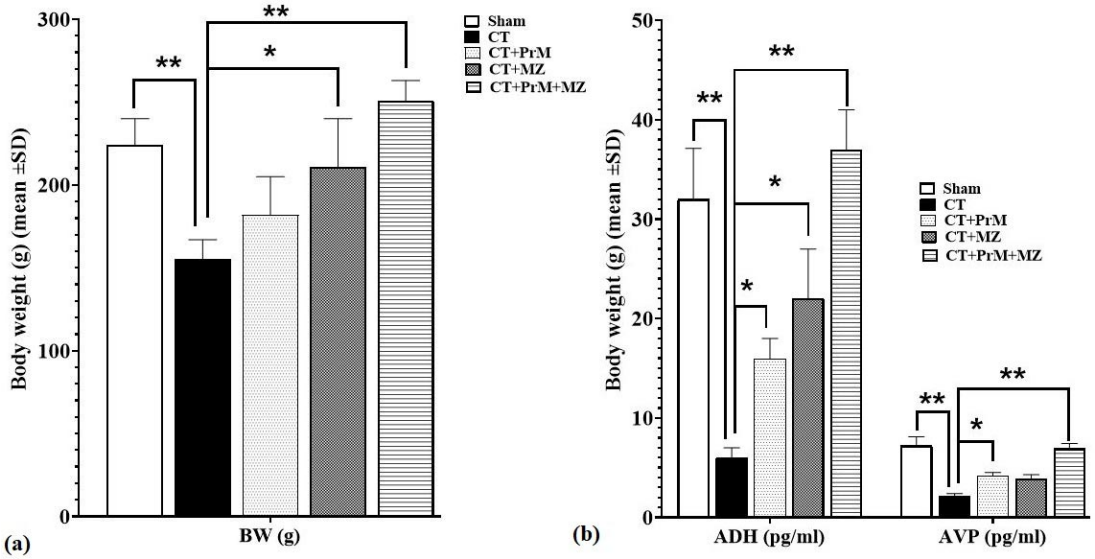

Fig. 2. (a) Rats body (g) weight and (b) Serum levels of ADH and AVP (pg/dl) (means ± SD; n=10/group) in experimental groups. * ($p<0.05$) and ** ($p<0.01$) significant differences between groups.

NO serum levels, along with serum activity of CAT, GPx, and SOD. CT, by triggering the production of free radicals, resulted in a significant ($p < 0.01$) increase in serum NO levels compared to the sham group. This was accompanied by a notable ($p < 0.01$) decrease in serum activity of CAT, GPx, and SOD. However, the study emphasized the potent antioxidant effects of MZ and PrM. MZ (in CT+ MZ group) significantly ($p < 0.05$) enhanced the serum activity of CAT, GPx, and SOD while simultaneously reducing NO levels compared to the CT group. Similarly, PrM (in CT+ PrM group) significantly ($p < 0.05$) increased serum GPx activity compared to the CT group. The most pronounced changes in serum antioxidant levels were observed in the CT+MZ+PrM co-treatment group, where the activities of all three endogenous antioxidants (CAT, GPx, and SOD) were significantly increased ($p < 0.01$), and serum NO levels were significantly reduced ($p < 0.01$) compared to the CT group (Fig. 3a).

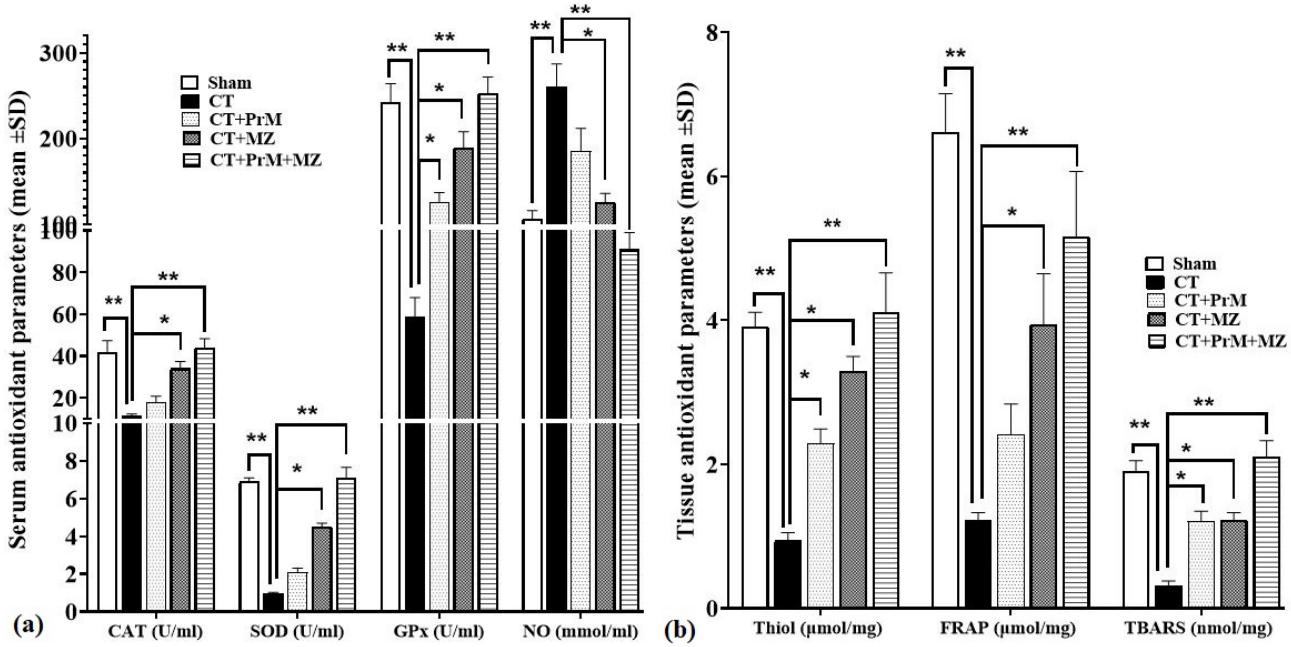

Fig. 3. (a) Serum levels of NO (mmol/ml), alongside the mean serum activity of SOD, CAT, and GPx (U/ml) and (b) intestine tissue levels of TBARS (nmol/mg) and FRAP (µmol/mg) (means ± SD; n=10/group) in experimental groups. * ($p<0.05$) and ** ($p<0.01$) significant differences between groups.

TBARS, thiol, and FRAP levels in intestine. TBARS, thiol, and FRAP levels, which serve as indicators of total antioxidant capacity and lipid peroxidation, were assessed in this study. Results showed that CT treatment significantly ($p < 0.01$) reduced tissue levels of all three markers compared to the sham group. Conversely, MZ and PrM, due to their high antioxidant capacity, significantly elevated ($p < 0.05$) the levels of these markers in the CT+MZ and CT+PrM groups compared to the CT group. The most substantial improvements in tissue antioxidant levels were observed in the CT+MZ+PrM co-treatment group, where TBARS, thiol, and FRAP levels in the intestine were significantly increased ($p < 0.01$) compared to the CT group (Fig. 3b).

Serum levels of IL-6, IL-10, TNF-α, and IL-1β. CT treatment induced inflammatory responses, resulting in elevated levels of pro-inflammatory cytokines and suppression of systemic anti-inflammatory cytokines. This led to a significant ($p < 0.01$) increase in serum levels of all three pro-inflammatory cytokines (IL-6, TNF-α, and IL-1β) compared to the sham group, along with a notable decrease in IL-10 levels. However, the study highlighted the potent anti-inflammatory effects of MZ and PrM. MZ (in CT+ MZ group)significantly ($p < 0.05$) increased serum IL-10 levels while simultaneously reducing the levels of all three pro-inflammatory cytokines (IL-6, TNF-α, and IL-1b) compared to the CT group. Similarly, PrM (in CT+ PrM group) significantly ($p < 0.05$) raised serum IL-10 levels while lowering IL-6 and IL-1β levels compared to the CT group. The most significant changes in serum cytokine levels were observed in the CT+MZ+PrM co-treatment group, where all three pro-inflammatory cytokines (IL-6, TNF-α, and IL-1β) were significantly reduced ($p < 0.01$), and serum IL-10 levels were significantly increased ($p < 0.01$) compared to the CT group (Fig. 4a).

Expression of intestine AQP3, AQP8, and AQP6 genes. A major factor contributing to osmotic imbalance in patients undergoing CT is the impairment of AQP functionality. The study demonstrated a significant reduction ($p < 0.01$) in the gene expression of all three AQPs (AQP3, AQP8, and AQP6) in the CT group compared to the sham group. MZ treatment (in the CT+MZ group) significantly ($p < 0.05$) elevated the intestinal expression of all three AQPs (AQP3, AQP8, and AQP6) compared to the CT group. Meanwhile, PrM treatment (in the CT+PrM group) significantly ($p < 0.05$) increased the intestinal expression of AQP3 compared to the CT group. The most notable enhancements in AQP gene expression were observed in the CT+MZ+PrM co-treatment group, where the expression of all three AQPs in the intestine was significantly elevated ($p < 0.01$) compared to the CT group (Fig. 4b).

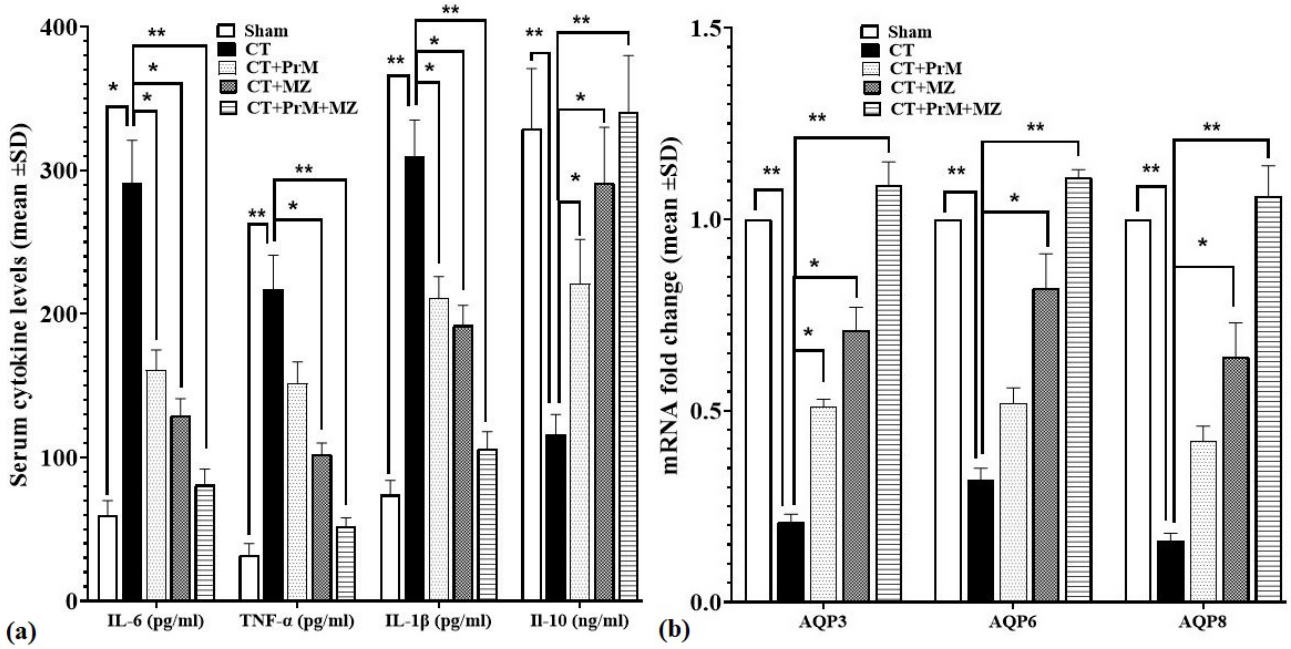

Fig. 4. (a) Serum levels of IL-6, IL-1β, TNF-α (pg/ml), and IL-10 (ng/ml) and (b) AQP3, AQP8, and AQP6 genes expression in intestine (means ± SD; n=10/group) in experimental groups. * ($p<0.05$) and ** ($p<0.01$) significant differences between groups.

Expression of intestine AQP3, AQP8, and AQP6 proteins. The study showed a significant decrease ($p < 0.01$) in the protein expression of all three AQPs (AQP3, AQP8, and AQP6) in the CT group compared to the sham group. Treatment with MZ (in the CT+MZ group) significantly ($p < 0.05$) increased the intestinal protein expression of all three AQPs (AQP3, AQP8, and AQP6) compared to the CT group. Additionally, PrM treatment (in the CT+PrM group) significantly ($p < 0.05$) raised the intestinal protein expression of AQP3 and AQP8 compared to the CT group. The most significant increases in AQP protein expression were observed in the CT+MZ+PrM co-treatment group, where the expression of all three AQPs in the intestine was markedly elevated ($p < 0.01$) compared to the CT group (Figs. 5a & 5b).

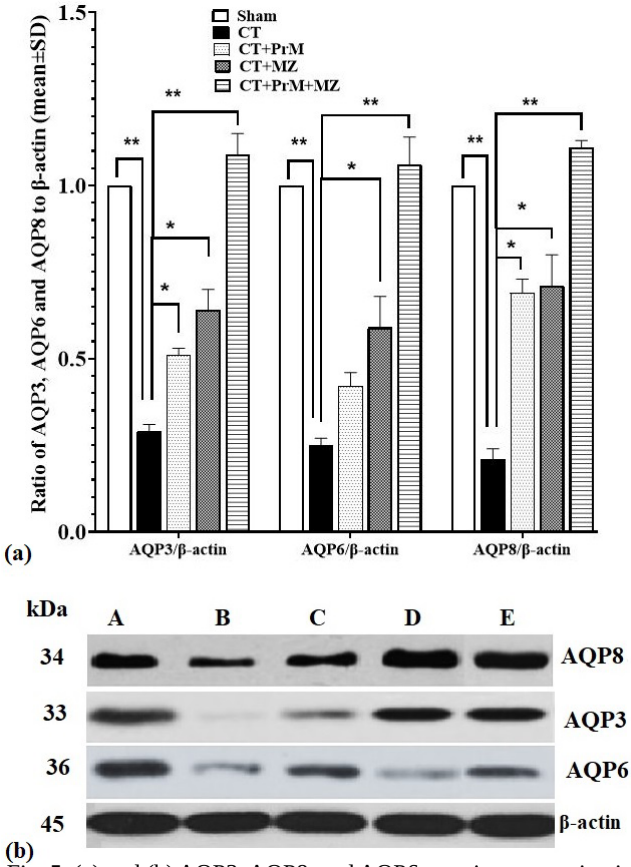

Fig. 5. (a) and (b) AQP3, AQP8, and AQP6 proteins expression in intestine (means ± SD; n=10/group) in experimental groups. * ($p<0.05$) and ** ($p<0.01$) significant differences between groups.

Intestine morphometrically and stereological evaluations . The study demonstrated a significant decrease ($p < 0.01$) in the thickness of the tunica mucosa and tunica muscularis, along with a significant increase ($p < 0.01$) in the thickness of the tunica submucosa and degenerative regions in the CT group compared to the sham group. Treatment with MZ (in the CT+MZ group) significantly ($p < 0.05$) increased the thickness of the tunica mucosa and tunica muscularis, while significantly decreasing the thickness of the tunica submucosa ($p < 0.05$) and degenerative regions ($p < 0.01$) compared to the CT group. Similarly, PrM treatment (in the CT+PrM group) significantly ($p < 0.05$) increased the thickness of the tunica mucosa and reduced the thickness of the tunica submucosa and degenerative regions compared to the CT group. The most pronounced improvements in intestinal layer thickness were observed in the CT+MZ+PrM co-treatment group, which showed significant increases in the thickness of the tunica mucosa and tunica muscularis and a notable decrease ($p < 0.01$) in the thickness of the tunica submucosa and degenerative regions compared to the CT group (Fig. 6 & Table II).

The study revealed a significant decrease ($p < 0.01$) in the volume of the tunica mucosa and a substantial increase ($p < 0.01$) in the volumes of the intestine, tunica submucosa, and degenerative regions in the CT group compared to the sham group. Treatment with MZ (in the CT+MZ group) significantly ($p < 0.05$) increased the volume of the tunica mucosa and significantly decreased the volumes of the intestine ($p < 0.05$), tunica submucosa ($p < 0.05$), and degenerative regions ($p < 0.01$) compared to the CT group. Similarly, PrM treatment (in the CT+PrM group) significantly ($p < 0.05$) increased the volume of the tunica mucosa and reduced the volumes of the tunica submucosa and degenerative regions compared to the CT group. The most pronounced improvements in intestinal layer volumes were observed in the CT+MZ+PrM co-treatment group, which showed significant increases in the volume of the tunica mucosa and notable decreases in the volumes of the intestine ($p < 0.05$), tunica submucosa ($p < 0.01$), and degenerative regions ($p < 0.01$) compared to the CT group (Fig. 6 & Table III).

Table. II. The thickness (μm) of layers in different layers of the intestine in experimental groups.

Groups	Tunica mucosa	Tunica submucosa	Tunica muscularis	Tunica serosa/ adventitia	Degenerating or lymphatic infiltration
Sham	143.6±8.1	21.6±3.1	156.1±9.2	4.1±0.91	0.26±0.03
CT	41.9±6.1**	81.6±9.1**	118.1±9.1*	5.1±0.81	21.2±4.2**
CT+PrM	81.4±6.2*	41.2±7.2*	123.7±9.11	4.6±0.62	14.21±1.2*
CT+MZ	102.7±10.4*	50.2±8.1*	142.7±5.9*	5.1±0.81	6.11±0.24**
CT+PrM+MZ	133.6±7.4**	69.4±3.6**	150.7±8.9*	4.6±0.23	2.61±0.91**

Data are presented as mean ± SD.

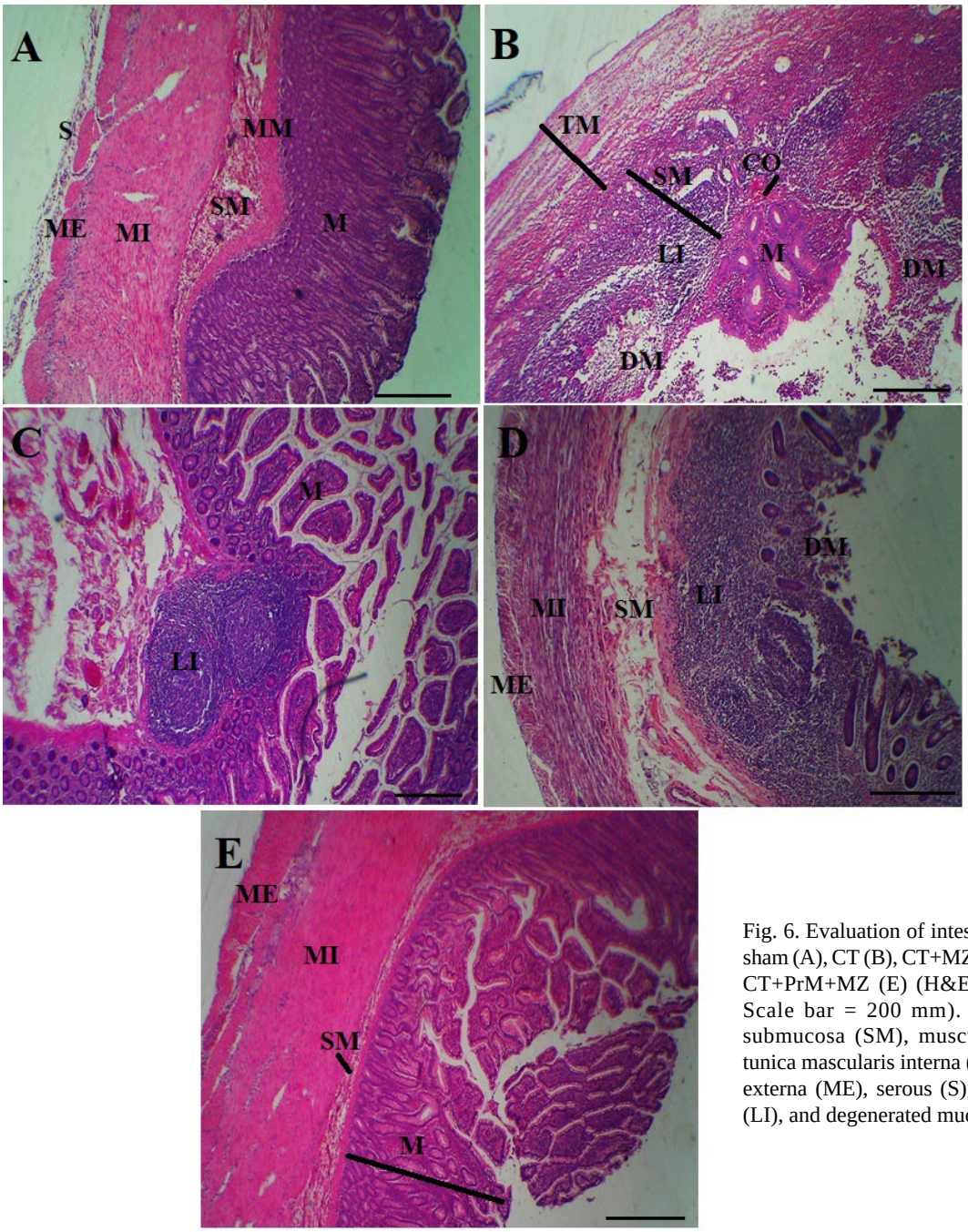

Fig. 6. Evaluation of intestinal histopathology in sham (A), CT (B), CT+MZ (C), CT+PrM (D), and CT+PrM+MZ (E) (H&E staining; × 100 with Scale bar = 200 mm). Tunica mucosa (M), submucosa (SM), muscularis mucosa (MM), tunica mascularis interna (MI), tunica mascularis externa (ME), serous (S), lymphatic infiltration (LI), and degenerated mucosa (DM).

Table. III. The values of volume (mm^3) of the intestine and its different layers in the in experimental groups.

Groups	Total volume	Tunica mucosa	Tunica submucosa	Tunica muscularis	Tunica serosa/ adventitia	Degenerating or lymphatic infiltration
Sham	323.6±19.1	151.7±9.4	44.7±6.4	142.6±6.4	7.2±0.6	1.23±0.4
CT	429.4±12.9*	67.21±9.2*	121.9±12.1**	141.7±11.3	6.9±0.7	61.4±10.2**
CT+PrM	391.8±11.9	121.4±8.1*	94.2±6.1*	161.4±10.4	5.9±0.91	33.4±8.2*
CT+MZ	369.9±16.1*	114.1±9.6*	50.2±8.1*	155.7±11.2	4.2±0.63	14.2±2.2**
CT+PrM+MZ	341.2±13.2*	132.4±7.9**	49.2±2.1*	149.7±6.2	5.2±0.93	3.2±0.9**

Data are presented as mean ± SD.

DISCUSSION

CT induced enterocolitis.This study highlights that CT and its metabolites induce enterocolitis in recipients through various mechanisms, including disruptions to ADH and AVP secretion pathways. Similar to other chemotherapy drugs, CT can alter ADH and AVP release, affecting fluid balance and causing electrolyte abnormalities. Prior research has shown that chemotherapeutic agents like cyclophosphamide and 5-FU can interfere with these hormone regulations, leading to fluid retention and hyponatremia, especially with highly emetogenic treatments (Li *et al*., 2024). CT also impacts gastrointestinal functions, such as mucositis and nausea, indirectly affecting ADH and AVP levels through altered fluid intake and absorption (Alzahrani *et al*., 2023). By the end of the study, CT treatment was shown to decrease serum levels of ADH and AVP. In addition, the generation of ROS and other free radicals by 5-FU and CT triggers oxidative stress, activating signaling pathways like NF-κB, MAPKs, the p53 pathway, and the PI3K/Akt pathway. These effects hinder cell proliferation and enhance apoptotic responses through pathways such as NF-κB/p53/Cas-3 and WNT/β-catenin(Agrawal *et al*., 2024). Furthermore, CT's interference with DNA synthesis disrupts enterocyte cell cycles, leading to cell cycle arrest in the G1 phase, which, in clinical settings, has resulted in severe diarrhea and disturbed electrolyte balance (Kalman, 2022). Animal studies have indicated that CT impairs antioxidant defenses by inhibiting enzymes such as GPx, CAT, and SOD, leading to intestinal mucosal damage and fluid imbalance (Xiao *et al*., 2024). This study observed a reduction in antioxidant capacity, as seen in decreased FRAP, TBARS, and thiol levels, along with increased NO levels. CT treatment also activated mitochondrial apoptotic pathways, elevating Bax, p53, and Caspase-3 expression while suppressing antioxidant enzymes. Patients undergoing CT experienced adverse gastrointestinal effects, such as severe diarrhea, mucositis, and enterocolitis, impacting treatment efficacy. Proposed strategies to mitigate these side effects include supplementation to restore electrolyte balance (Li *et al*., 2024). Notably, CT also disrupts AQPs, specifically AQP3, AQP8, and AQP6, in intestinal cells, hindering water transport and further contributing to gastrointestinal dysfunction through apoptosis induction and impaired AQP expression and repair, particularly through the p53-dependent apoptotic pathway.

MZ and PrM ameliorates enterocolitis induced by CT. The current investigation highlights the mitigating effects of MZ and PrM on CT-induced enterocolitis, with a particularly notable synergistic ameliorative impact. This beneficial outcome is driven by diverse mechanisms.

In contemporary medicine, MZ serves as a first-line therapy for achieving and maintaining remission in mild to moderate cases of ulcerative colitis and Crohn's disease, frequently administered post-surgery to prevent recurrence (S?oka *et al*., 2023). Its action is primarily topical on the colonic mucosa, where it inhibits pro-inflammatory cytokines, reduces oxidative stress, and modulates immune responses (Beiranvand, 2021). Preclinical studies have demonstrated MZ's ability to suppress nuclear factor-kappa B (NF-κB), a key mediator of inflammation, and reduce the expression of inflammatory enzymes such as cyclooxygenase-2 (COX-2) and inducible nitric oxide synthase (iNOS) in enterocytes during chemotherapy. MZ's antioxidative properties involve enhancing the activity of enzymes like SOD, GPx, and CAT, mitigating ROS and preserving intestinal mucosa integrity (Movahedinia *et al*., 2021). In animal models, including murine studies, MZ has been shown to significantly reduce oxidative damage markers, preserve intestinal tissue integrity, and counteract lipid peroxidation (Li *et al*., 2021). Beiranvand and Bahramikia (2020), demonstrated that MZ mitigated mucosal damage in ethanol-induced gastric ulcers by boosting antioxidant enzyme activity and protecting against apoptosis in parietal and zymogenic cells (Beiranvand & Bahramikia, 2020). In this study, MZ increased intestinal antioxidant capacity, reduced lipid peroxidation, and elevated serum levels of SOD, GPx, and CAT. Additionally, MZ exhibited potent anti-inflammatory effects, suppressing pro-inflammatory cytokines like IL-6, IL-1β, and TNF-α while enhancing anti-inflammatory cytokines, particularly IL-10. MZ has also shown efficacy in combination with probiotics such as *Lactobacillus casei*, reducing inflammatory markers in animal models of colitis. Studies by Subramanian *et al*. (2008), further supported its role in preserving mucosal integrity by inhibiting epithelial IL-8 responses (Subramanian *et al*., 2008). Beyond anti-inflammatory actions, MZ positively influences AQPs, crucial for intestinal water transport, by normalizing AQP3, AQP6, and AQP10 expression (Bozkurt *et al*., 2023). This regulation enhances fluid balance and intestinal osmolarity, countering the adverse effects of chemotherapy-induced diarrhea and dehydration through modulation of the ADH and AVP pathways. These findings suggest that MZ holds substantial therapeutic promise for managing chemotherapy-related gastrointestinal complications, warranting further exploration in both clinical and preclinical settings.

Probiotic mixtures (PrM) have shown considerable promise in supporting gastrointestinal health, particularly for conditions such as ulcerative colitis and enterocolitis. These probiotics contribute to gut health by improving digestion, regulating immune responses, and promoting mucosal healing while restoring balance to the gut

microbiota (Gu *et al*., 2022). Their therapeutic effects are mediated through various molecular pathways, including apoptosis regulation, inhibition of the NF-κB pathway to reduce inflammation, modulation of the MAPK pathway, and activation of the PI3K/Akt/mTOR pathway to promote cell survival and growth (Han *et al*., 2021). Clinical studies in both human and animal models have demonstrated that these probiotics can alleviate symptoms, reduce inflammatory markers, and improve overall quality of life, signaling their therapeutic potential, although further research is needed to better understand their mechanisms and optimize their use (Kobyliak *et al*., 2018).

Dashtbanei and Keshtmand (2023), explored the effects of a multi-strain probiotic mixture containing *Lactobacillus rhamnosus* and *Lactobacillus helveticus* on oxidative injuries in the small intestine of rats exposed to cadmium. Their findings highlighted that this PrM suppressed the secretion of pro-inflammatory cytokines IL-8 and TNF-a, thereby inhibiting enterocyte apoptosis and preventing intestinal mucosal degeneration, indicating a protective role against oxidative damage (Dashtbanei & Keshtmand, 2023). In another study by Kohan and Keshtmand (2024), a probiotic mixture containing *Lactobacillus casei* and *Lactobacillus rhamnosus* was shown to enhance liver antioxidant capacity, reduce lipid peroxidation, and increase serum levels of antioxidant enzymes like SOD, GPx, and CAT (Kohan & Keshtmand, 2024). This PrM effectively protected hepatocytes from apoptosis, providing a potential therapeutic approach for mitigating cadmium-induced liver damage. In the current study, the synergy between PrM and MZ significantly boosted antioxidant capacity (measured by FRAP, TBARS, and thiol) and enhanced antioxidant enzyme activity (SOD, GPx, and CAT). It also reduced tissue and systemic free radical levels (NO), alleviating inflammatory pathways and the release of cytokines like IL-6, TNF-α, and IL-1β.

CONCLUSION

MZ and PrM demonstrate synergistic protective effects against CT-induced enterocolitis. Both MZ and PrM have antioxidant, anti-inflammatory, and anticancer properties that help safeguard normal cells while inhibiting tumor progression. These findings suggest that a commercial prodrug derived from MZ and PrM could be beneficial for cancer patients. However, further research is necessary to explore their broader effects and additional protective mechanisms across different human and animal models.

Ethical Approval . The experimental protocols of this study were approved by the Wuhan Eighth Hospital (Wuhan Anorectal Hospital) ethics committee.

CHE, H.; XU, Y.; HUANG, Y. & GUO, Z. Efectos protectores de los probióticos y la mesalazina contra la enterocolitis inducida por capecitabina en ratas: Una investigación bioquímica, molecular, estereológica e histopatológica. *Int. J. Morphol., 43(2)*:458-469, 2025.

RESUMEN: Este estudio tuvo como objetivo explorar los efectos protectores de una mezcla probiótica (PrM) compuesta por *Lactobacillus casei*, *Lactobacillus rhamnosus* y *Lactobacillus helveticus*, junto con mesalazina (MZ), contra la enterocolitis inducida por capecitabina (CT). La investigación se llevó a cabo utilizando una combinación de análisis bioquímicos, moleculares e histopatológicos. Se asignaron al azar cincuenta ratas Wistar a cinco grupos (10 ratas cada uno) y se las monitoreó durante un período de 50 días. Los grupos incluyeron un grupo de simulación, un grupo de solo CT, un grupo que recibió CT y MZ (50 mg/kg), un grupo que recibió CT y PrM (10 mg/kg) y un grupo de co-tratamiento que recibió CT, MZ y PrM. El día 51, después de la eutanasia, se recogieron muestras de sangre de los corazones de las ratas para su posterior análisis. Se midieron los niveles séricos de óxido nítrico, así como la actividad de enzimas antioxidantes como la catalasa, la glutatión peroxidasa y la superóxido dismutasa. También se evaluaron las concentraciones séricas de hormona antidiurética (ADH) y arginina vasopresina (AVP). Se evaluaron los marcadores de estrés oxidativo en el tejido intestinal, incluidos FRAP, tiol y TBARS. Los niveles de citocinas proinflamatorias, como la interleucina-6 (IL-6), el factor de necrosis tumoral-α (TNF-α), la interleucina-1β (IL-1β) y la IL-10 se cuantificaron mediante ELISA. La homeostasis del agua en el intestino se investigó examinando la expresión de los genes de las acuaporinas (AQP) (AQP3, AQP8 y AQP6) mediante PCR en tiempo real, mientras que la expresión de proteínas se determinó mediante transferencia Western. Además, se evaluó la integridad estructural del tejido intestinal en los grupos de estudio mediante una evaluación histopatológica. Se descubrió que los tratamientos con MZ y PrM reducían la apoptosis de las células intestinales y regulaban positivamente la expresión de los genes y proteínas de las AQP intestinales al mejorar la actividad de las enzimas antioxidantes y reducir los niveles de radicales libres. El tratamiento combinado también demostró un efecto sinérgico en la modulación de los niveles de citocinas proinflamatorias y la regulación de la ADH y la AVP, lo que contribuye al mantenimiento del equilibrio osmótico sérico e intestinal. El estudio sugiere que la MZ y la PrM tienen beneficios terapéuticos potenciales para el manejo de la enterocolitis en pacientes sometidos a quimioterapia al mitigar el estrés oxidativo, reducir la inflamación y preservar la homeostasis hídrica intestinal.

PALABRAS CLAVE: Probiótico; Mesalazina; Capecitabina; Intestino; Enterocolitis; Apoptosis.

REFERENCES

Agrawal, S.; Lee, C.; Pierce, W. F.; Everhart, E.; King-Ducre, A.; Royce, M.; Osgood, C. L.; Amiri-Kordestani, L.; Chiu, H. J.; Ricks, T. K.; et al. FDA approval summary: capecitabine labeling update under project renewal. *Clin. Cancer Res., 30(24)*:5508-14, 2024.

Alzahrani, S. M.; Al Doghaither, H. A.; Al-Ghafari, A. B. & Pushparaj, P. N. 5-Fluorouracil and capecitabine therapies for the treatment of colorectal cancer. *Oncol. Rep., 50(4)*:175, 2023.

Beiranvand, M. A review of the biological and pharmacological activities of mesalazine or 5-aminosalicylic acid (5-ASA): an anti-ulcer and anti-oxidant drug. *Inflammopharmacology, 29(5)*:1279-90, 2021.

Beiranvand, M. & Bahramikia, S. Ameliorating and protective effects mesalazine on ethanol-induced gastric ulcers in experimental rats. *Eur. J. Pharmacol., 888*:173573, 2020.

Bojarzadeh, H.; Sadeghinezhad, J.; Bahrami, M. M. & Shahipour, M. R. Volumetric study on small intestine in newborn rat using design-based stereology technique. *Int. J. Vet. Sci. Res., 4(2)*:35-40, 2024.

Bozkurt, A.; Halici, H. & Yayla, M. Aquaporins: potential targets in inflammatory diseases. *Eurasian J. Med., 55(Suppl. 1)*:S106-S113, 2023.

Cai, Z.; Shen, Z.; Zhao, J.; Zhang, H.; Guo, Z.; Xia, Q.; Liang, H.; Liu, J.; Tan, L.; Sheng, H.; et al. AQP8 may affect glioma proliferation and growth by regulating GSK-3b phosphorylation and nuclear transport of b-catenin. *Int. J. Dev. Neurosci., 83(4)*:333-45, 2023.

D'Amico, F.; Parigi, T. L.; Fiorino, G.; Peyrin-Biroulet, L. & Danese, S. Tofacitinib in the treatment of ulcerative colitis: efficacy and safety from clinical trials to real-world experience. *Therap. Adv. Gastroenterol.,12*:1756284819848631, 2019.

Dashtbanei, S. & Keshtmand, Z. A mixture of multi-strain probiotics (*Lactobacillus rhamnosus*, *Lactobacillus helveticus*, and *Lactobacillus casei*) had anti-inflammatory, anti-apoptotic, and anti-oxidative effects in oxidative injuries induced by cadmium in small intestine and lung. *Probiotics Antimicrob. Proteins, 15(2)*:226-38, 2023.

Golosova, D. V.; Shakhmatova, E. I. & Natochin, Y. V. Differences between arginine-vasotocin and arginine-vasopressin effects on the rat kidney in evolution of osmoregulation in vertebrates. *J. Evol. Biochem. Phys., 55(1)*:71-9, 2019.

Goodarzi, N.; Akbari Bazm, M.; Naseri, L. & Hosseinipour, M. Histomorphometrical and stereological study of the oesophagus in the adult male Persian squirrel (Sciurus anomalus). Anat. Histol. Embryol., 48(5):444-8, 2019.

Gu, Q.; Yin, Y.; Yan, X.; Liu, X.; Liu, F. & McClements, D. J. Encapsulation of multiple probiotics, synbiotics, or nutrabiotics for improved health effects: A review. *Adv. Colloid Interface Sci., 309*:102781, 2022.

Han, S.; Lu, Y.; Xie, J.; Fei, Y.; Zheng, G.; Wang, Z.; Liu, J.; Lv, L.; Ling, Z.; Berglund, B.; et al. Probiotic gastrointestinal transit and colonization after oral administration: A long journey. *Front. Cell. Infect. Microbiol., 11*:609722, 2021.

Kalman, T. I. Rational design of an orally active anticancer fluoropyrimidine, pencitabine, a hybrid of capecitabine and gemcitabine. *ACS Med. Chem. Lett., 13(3)*:409-16, 2022.

Kobyliak, N.; Falalyeyeva, T.; Mykhalchyshyn, G.; Kyriienko, D. & Komissarenko, I. Effect of a live probiotic on insulin resistance in type 2 diabetes patients: randomized clinical trial. *Diabetes Metab. Syndr. Clin. Res. Rev., 12(5)*:617-24, 2018.

Kohan, A. & Keshtmand, Z. Ameliorating effects of Lactobacillus probiotics on cadmium-induced hepatotoxicity, inflammation, and oxidative stress in Wistar rats. *Comp. Clin. Pathol., 33*:653-64, 2024.

Li, B.; Du, P.; Du, Y.; Zhao, D.; Cai, Y.; Yang, Q. & Guo, Z. Luteolin alleviates inflammation and modulates gut microbiota in ulcerative colitis rats. *Life Sci., 269*:119008, 2021.

Li, L.; Tan, H. & Su, T. Fraxinus excelsior L. for prevention of capecitabine-induced enterocolitis in rat: an integrated biochemical, molecular, and histopathological study. *Pharmacogn. Mag., 20(4)*:1086-99, 2024.

Loya-Zurita, R. E.; Gersenowies-Rodríguez, J. R.; Olvera-Ramos, J. A. & Pérez-Bautista, D. S. Morphometric comparison of transparent skeletons of four species of myomorphic rodents. *Int. J. Morphol., 42(1)*:107-10, 2024.

Meshkibaf, M. H.; Maleknia, M. & Noroozi, S. Effect of curcumin on gene expression and protein level of methionine sulfoxide reductase A (MSRA), SOD, CAT and GPx in Freund's adjuvant inflammation-induced male rats. *J. Inflamm. Res., 12*:241-9, 2019.

Movahedinia, H.; Shahidi-Zandi, M. & Kazemipour, M. Investigation of 5-aminosalicylic acid (mesalazine drug) as a corrosion inhibitor for carbon steel in sulfuric acid solution. *Int. J. Electrochem., 16(2)*:210228, 2021.

Sloka, J.; Madej, M. & Strzalka-Mrozik, B. Molecular mechanisms of the antitumor effects of mesalazine and its preventive potential in colorectal cancer. *Molecules, 28(13)*:5081, 2023.

Subramanian, S.; Rhodes, J. M.; Hart, A. C.; Tam, B.; Roberts, C. L.; Smith, S. L.; Corkill, J. E.; Winstanley, C.; Virji, M. & Campbell, B. J. Characterization of epithelial IL-8 response to inflammatory bowel disease mucosal E. coli and its inhibition by mesalamine. *Inflamm. Bowel Dis., 14(2)*:162-75, 2008.

Wang, L.; Wang, R.; Wei, G. Y.; Zhang, R. P.; Zhu, Y.; Wang, Z.; Wang, S. M. & Du, G. H. Cryptotanshinone alleviates chemotherapy-induced colitis in mice with colon cancer via regulating fecal-bacteria-related lipid metabolism. *Pharmacol. Res., 163*:105232, 2021.

Xiao, P.; Ma, H.; Kuang, C. & Wang, W. Hydroalcoholic extract of Lepidium draba L. ameliorates capecitabine-induced enterocolitis in rats. *J. Anim. Plant Sci., 34(4)*:999-1011, 2024.

Yarahmadzehi, S.; Fanaei, H.; Mirshekar, M. A. & Atashpanjeh, A. R. Opium consumption exerts protective effect against cerebral ischemia through reducing inflammation and enhancing antioxidant defense in male rats. *Neurol. Psychiat. Brain Res., 37*:15-20, 2020.

Yu, P.; Wang, X.; Xie, Y.; Zhang, H. & Zhang, F. Activatable NIR-II lanthanides-polymetallic oxomolybdate hybrid nanosensors for monitoring chemotherapy induced enteritis. *Adv. Funct. Mater., 33(36)*:2301683, 2023.

Zogbi, C.; Oliveira, N. C.; Levy, D.; Bydlowski, S. P.; Bassaneze, V.; Neri, E. A. & Krieger, J. E. Beneficial effects of IL-4 and IL-6 on rat neonatal target cardiac cells. *Sci. Rep., 10(1)*:12350, 2020.

Corresponding author:
Dr. Zhiwei Guo
Department of Anorectal
Wuhan Eighth Hospital (Wuhan Anorectal Hospital)
Wuhan, 430030
CHINA

E-mail: gzw72197908@sina.com

ORCID: https://orcid.org/0009-0007-8300-2069